DEVELOPMENTAL BIOLOGY

Primary specification of blastocyst trophectoderm by scRNA-seq: New insights into embryo implantation

Dandan Liu[1,2,3]†, Yidong Chen[1,2,3,4,5]†, Yixin Ren[1,2,3]†, Peng Yuan[1,2], Nan Wang[1,3], Qiang Liu[1,2], Cen Yang[1,2], Zhiqiang Yan[1,2], Ming Yang[1,4,5], Jing Wang[1,2], Ying Lian[1], Jie Yan[1,2], Fan Zhai[1,2], Yanli Nie[1,2], Xiaohui Zhu[1,2], Yuan Chen[1], Rong Li[1,2], Hsun-Ming Chang[1], Peter C. K. Leung[1], Jie Qiao[1,2,3,4,5,6]*, Liying Yan[1,2]*

Mechanisms of implantation such as determination of the attachment pole, fetal-maternal communication, and underlying causes of implantation failure are largely unexplored. Here, we performed single-cell RNA sequencing on peri-implantation embryos from both humans and mice to explore trophectoderm (TE) development and embryo-endometrium cross-talk. We found that the transcriptomes of polar and mural TE diverged after embryos hatched from the zona pellucida in both species, with polar TE being more mature than mural TE. The implantation poles show similarities in cell cycle activities, as well as in expression of genes critical for implantation and placentation. Embryos that either fail to attach in vitro or fail to implant in vivo show abnormalities in pathways related to energy production, protein metabolism, and 18*S* ribosomal RNA m^{6}A methylation. These findings uncover the gene expression characteristics of humans and mice TE differentiation during the peri-implantation period and provide new insights into embryo implantation.

INTRODUCTION

In mammals, successful implantation is the basis of pregnancy establishment. However, even genetically normal blastocysts fail to implant at a rate of 40 to 50% (*1*). During implantation, the outer layer of blastocyst cells, namely, the trophectoderm (TE), develops into the trophoblast lineage that directly attaches to and invades a synchronized endometrium (*2*). Any abnormalities in either the embryo or the endometrium will result in implantation failure. Compared to the effects of endometrial factors, the impact of blastocyst TE on gestational outcomes has long been underestimated (*3*). However, there has been growing interest in studies of the correlation between TE cell development and implantation in recent years. During the blastocyst stage, the embryo polarizes with its compact inner cell mass (ICM) surrounded by a monolayer of TE moving to one side. Despite the long-held notion that the entire TE layer has an equal potential to interact with the endometrium and to form an implantation site (*4*), it has recently been increasingly recognized that the polar and mural TE cells are different in their potentials (*5*, *6*). In species such as pigs, horses, guinea pigs, mice, and rats, the embryo consistently orients itself toward, attaches to, and invades the endometrium via the mural TE (*7*, *8*). In humans and nonhuman primates, however, it is the polar TE that attaches to the endometrium (*9*, *10*). Mouse models have been used as powerful tools to study embryo implantation. However, the differential mechanisms underlying TE cell development and implantation initiation in mice and humans remain elusive.

[1]Center for Reproductive Medicine, Department of Obstetrics and Gynecology, Peking University Third Hospital, Beijing 100191, China. [2]National Clinical Research Center for Obstetrics and Gynecology, Beijing 100191, China. [3]Key Laboratory of Assisted Reproduction (Peking University), Ministry of Education, Beijing 100191, China. [4]Beijing Advanced Innovation Center for Genomics, Beijing 100871, China. [5]Peking-Tsinghua Center for Life Sciences, Peking University, Beijing 100871, China. [6]Beijing Key Laboratory of Reproductive Endocrinology and Assisted Reproductive Technology, Beijing 100191, China.
*Corresponding author. Email: yanliyingkind@aliyun.com (L.Y.); jie.qiao@263.net (J.Q.)
†These authors contributed equally to this work.

At present, it remains unclear how mural and polar TEs play their roles in anchoring the embryo to the endometrium. Because of the inaccessibility of in vivo experimentation at the attachment stage, in vitro models have become vital tools to investigate embryo development and cell-cell cross-talk at the implantation site. Post-implantation embryo culture systems have been established in the absence of maternal tissues. In certain conditioned culture medium, embryos can be attached to the culture dish on day 7, the same time they normally implant in vivo, and the cultured embryos can autonomously organize themselves for further development (*11*). This model of cultured human embryos from the preimplantation period to the postimplantation period has been applied to investigate TE cell development during early implantation (*12*). However, this model is not detailed enough to investigate embryo-endometrium interaction. Because of the limited accessibility of primary human endometrial epithelial cells, the endometrial adenocarcinoma–derived Ishikawa (ISK) cell line has become a powerful tool to study embryo implantation. Coculture of mouse or human embryos with ISK cells was previously described (*13*, *14*), enabling the exploration of human embryo-endometrium cross-talk. Recent single-cell transcriptome studies have provided abundant data on the specification of three lineages, including epiblast (EPI), primitive endoderm (PE), and TE, in preimplantation human embryos and extensively analyzed the differentiation of blastocyst TE (*5*, *6*, *15*–*17*). Specifically, single-cell RNA sequencing (scRNA-seq) was used to analyze trophoblast differentiation at the postattachment stage (from days 8 to 12) (*18*) and in first-/second-trimester human placentas (*19*). Another study showed that TE transcription patterns shifted from days 6 to 14, and trophoblast subpopulations were defined (*20*). However, more detailed information is needed regarding the TE cell sublineage during the periattachment stage.

This study focused on TE cell development from the preimplantation stage to attachment to ISK cells in vitro. scRNA-seq analysis has been applied to investigate human and mouse peri-implantation embryo cells obtained from physically dissected polar and mural poles to classify the subpopulations of TE cells. We aimed to elucidate the

gene expression characteristics of polar and mural TE cells at different developmental stages. Upon the establishment of an embryo–endometrial cell coculture system, we investigated cell-cell interactions between TE and endometrial cells and observed the functional roles of different TE sublineages in embryo implantation. We further examined the factors that may cause implantation failure by comparing the characteristics of embryos that failed to attach to the endometrium in vitro with those of embryos that failed to implant in vivo.

RESULTS

In this study, we collected both human and mouse embryos during the preimplantation stage. Human embryos were donated by patients undergoing in vitro fertilization (IVF) treatment, and all participants signed an informed consent form. To simplify the stage presentations of embryos from humans and mice, blastocysts with an intact zona pellucida [B3 and B4 embryos in Gardner grading, days 5 and 6 in humans and embryonic day 3.5 (E3.5) in mice] were defined as stage I (S1), and completely hatched B6 embryos (days 6 and 7 in humans and E4.5 in mice) were defined as stage II (S2). Hatched blastocysts cocultured with ISK cells for 24 hours (days 7 and 8 in humans and E5.5 in mice) were defined as stage III (S3) (Fig. 1, A and B). Each embryo was dissected into two parts with a laser (under microscopic guidance) along the edge of the ICM (Fig. 1, C to E). Human embryos attached to ISK cells on the polar side, similar to that in vivo (Fig. 1F). Before laser dissection, S3 embryos were carefully removed by detaching the cells around the attachment site. Clusters of polar and mural cells were further separated into individual single cells via enzyme digestion for scRNA-seq. Cell aggregates from the polar poles were composed of a mixture of the ICM, TE, and cocultured Ishikawa cells (coISK), while the mural poles were composed of practically pure TE cells (Fig. 1, C to E).

After the exclusion of cells that failed to meet certain data quality thresholds, a total of 2327 individual cells were analyzed in this

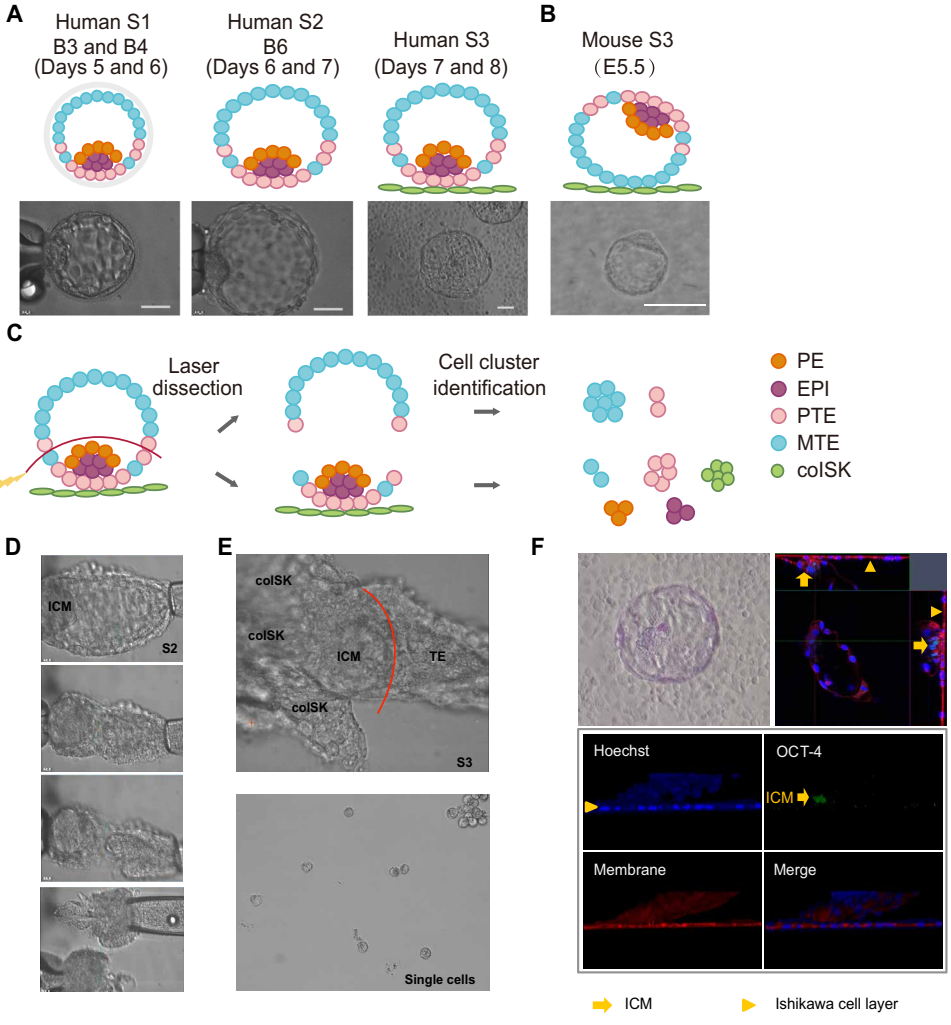

Fig. 1. scRNA-seq transcriptome profiling of peri-implantation embryos. (**A**) Representative images of three human embryonic stages. Left: Stage I, B3 and B4, days 5 and 6, blastocyst with zona. Middle: Stage II, B6, days 6 and 7, hatched blastocyst. Right: Stage III, days 7 and 8, hatched blastocyst cocultured with ISK cells for 24 hours and attached to ISK cells. Scale bar, 50 μm. (**B**) Representative images of mouse stage III embryo. Scale bars, 100 μm. (**C**) Schematic illustration of TE cell subtype identification. Blue cell: MTE, pink cell: PTE, orange cell: PE, purple cell: EPI, and green cell: coISK. (**D** and **E**) Process of dissecting S2 (D) and S3 (E) embryos under microscopy by laser and digested single cells. The red line shows the cutting path. (**F**) Immunofluorescence images show the embryo–endometrial cell coculture system (human embryo).

study (fig. S1A). Among these cells, a total of 1719 cells from human and mouse embryos (S1 to S3), including ISK cells, were analyzed for TE development and cell-cell cross-talk; 163 cells from two partially hatched (B5) human blastocysts were retained to analyze the cells at the hatching site, and 437 cells from four embryos with attachment failure (AF) and 8 cells biopsied from embryos for preimplantation genetic testing were used for implantation failure analysis.

Development and differentiation of human TE cells

A total of 25 human embryos, comprising 8 S1 embryos, 12 S2 embryos, and 5 S3 embryos (embryos that failed to attach were excluded), were collected along with two clusters of coISK; all samples were analyzed for human TE cell differentiation (fig. S1A). On average, 7077 genes and 0.7 million transcripts were expressed in each cell (fig. S1, B and C, and table S1). Unsupervised hierarchical clustering results showed that cells from the same developmental stage were clustered together, excluding cells from a few embryos that may have been in transitional developmental stages. Cells from the same pole were closer than those from different poles within each stage (fig. S1D). Principal components analysis (PCA) revealed that cells presented stage continuity (fig. S1E). Uniform manifold approximation and projection (UMAP) showed distinct clusters of TE, ICM, and coISK. As expected, all ICM cells were specifically located in the embryonic pole (fig. S1F). Different cell types could be distinguished by the expression of certain marker genes, such as *CDX2*, *GATA2*, and *GATA3* for TE; *SOX2*, *NANOG*, and *POU5F1* for EPI; and *GATA4*, *PDGFRA*, and *FOXA2* for PE (*5*, *15*). The ISK cells that adhered to the embryos were distinguished from embryonic cells by clustering with experimental labeled coISK cells (fig. S1, F and G).

Gene Ontology (GO) analysis was performed to identify the signatures most strongly associated with each stage of TE (fig. S2A and table S2). S1 TE cells were active in metabolism, energy production, and the assembly of cell-cell junctions, contributing to the development of a functional outer TE layer on the blastocyst. S2 TE cells were active in nitrogen compound biosynthetic processes and vitamin metabolic processes, especially folic acid metabolism. For S3 TE, the top GO terms were translational elongation, cell proliferation, blood vessel development, and hormonal responses. As determined by the gene expression tendencies, nine clusters of differentially expressed genes (DEGs) were classified in S1 to S3 TE (fig. S2B). Among these DEGs, the expression of *ESRRB*, which is required for mouse trophoblast stem cell self-renewal, and the pluripotency marker gene *POU5F1* (*21*, *22*) were decreased as TE cells developed. The placental development genes *DLX3*, *RXRA*, and *PPARG* (*23*–*25*) were increasingly expressed in TE cells with embryo development. Cell cycle genes that regulated the G_1-S transition, including *CCNE1* and *CDK2*, were up-regulated in S3 TE cells, while those controlling the G_2-M transition, including *CCNB1* and *CDK1*, were down-regulated, suggesting that DNA replication increased while cell division decreased in S3 TE cells (fig. S2C).

Human blastocysts are consistently attached to endometrial cells by the polar side (*10*). To comprehend the differences between TE cells from the polar and mural sides, we physically dissected the embryos with a laser to separate the polar part from the mural part. ICM and TE cells were clearly distinguished by cell clustering at all three stages (Fig. 2A) and defined by traditional marker genes (fig. S3A). At stage I, no obvious subtypes were observed among the TE cells. At stage II, four TE subtypes were identified. Combining location information, the cell type found mostly in the polar part was characterized as PTE (polar TE), and the type found mostly in the mural part was defined as MTE (mural TE). Because the boundary between polar and mural TEs is blurry, both PTE and MTE included small numbers of cells from the other side. The following analyses were based on clustered cell types instead of cell locations. Three subclusters of MTEs were observed at stage II. Among the three subgroups of MTEs, the gene expression profiles of MTE1 and MTE2 were similar, while that of MTE3 was closer to that of PTE (Fig. 2B and table S3). Pseudotime analysis of S2 TEs showed that S2 PTE was more mature than S2 MTE, as S2 PTE was at the end of the trajectory. The developmental stage of MTE3 was between those of MTE1/2 and PTE, indicating that MTE3 represents a transitional state (fig. S3B). We merged our S2 embryo datasets with the corresponding stage of embryos (embryonic days 6 and 7) from a previous study (*5*), and the distribution of cells from the two studies were mixed very well (Fig. 2A). The cell types of S2 PTE and three S2 MTEs were further verified by comparison with the datasets from this study (fig. S3, C and D). When cocultured with ISK cells for 24 hours, TE cells can be clearly divided into PTE and MTE (Fig. 2A). Specifically, PTE started to prepare for placental development by enriching genes involved in cellular responses to hormone stimuli and blood vessel development. MTE, however, was more active in energy metabolism (fig. S4A). The gene expression patterns of S2 PTE and S3 PTE were very similar in regard to cell motion, in utero embryonic development, and hormonal responses (Fig. 2B). Genes related to metabolism and cell cycle regulation, however, showed different expression patterns. The cell cycle was less active in PTE than in MTE. Notably, the cell cycle was even more inactive in S3 PTE than in S2 PTE (fig. S4, B to D). Thus, it appears that the transcriptome of PTE and MTE have become distinct after hatching from the zona pellucida, with PTE being the more mature of the two (Fig. 2C). All the cell types were consistent when merging all the three stages' cells together (fig. S3E).

For the partially hatched embryos, the hatching site could be located on either the mural side or the polar side. To determine whether the TE cells at the hatching site were more advanced, we included two more embryos that were partially hatched (B5 by the Gardner scoring system). We analyzed transcriptome of MTE cells from the hatching site and nonhatching site. PCA showed that these two embryos were between S1 and S2 in regard to their developmental stages, and the characteristics of MTE cells at the hatching site were equivalent to that in the nonhatching site (fig. S4E).

ATP6V0D2 (ATPase H^+ transporting V0 subunit d2), which regulates H^+ transport, is vital for blastocyst cavity formation. CYP26A1 (cytochrome P450 family 26 subfamily A member 1) is a critical enzyme that regulates the metabolism of retinoic acid and is involved in the processes of embryonic development, cell differentiation, and embryo implantation (*26*, *27*). Both *ATP6V0D2* and *CYP26A1* were highly expressed in S1 TE cells (Fig. 2, D and E). Notably, traditional TE markers were not equally expressed in MTE and PTE. For example, *HAND1* (*28*) was preferentially expressed in MTE (Fig. 2, D and E), and villous syncytiotrophoblast (STB) marker genes, including *SDC1*, *GCM1*, *OVOL1*, *ERVFRD-1*, and *CGA* (*29*–*31*), were up-regulated in S2 PTE and S3 PTE (Fig. 2, D and E, and figs. S4F and S5A). Multinucleated cells were observed at the polar TE in human B6 embryos (fig. S5B). Moreover, *PGF* (placenta growth factor, a gene regulated by *GCM1*) (*32*) was also highly expressed in S2 and S3 PTEs, presumably supporting embryo attachment and

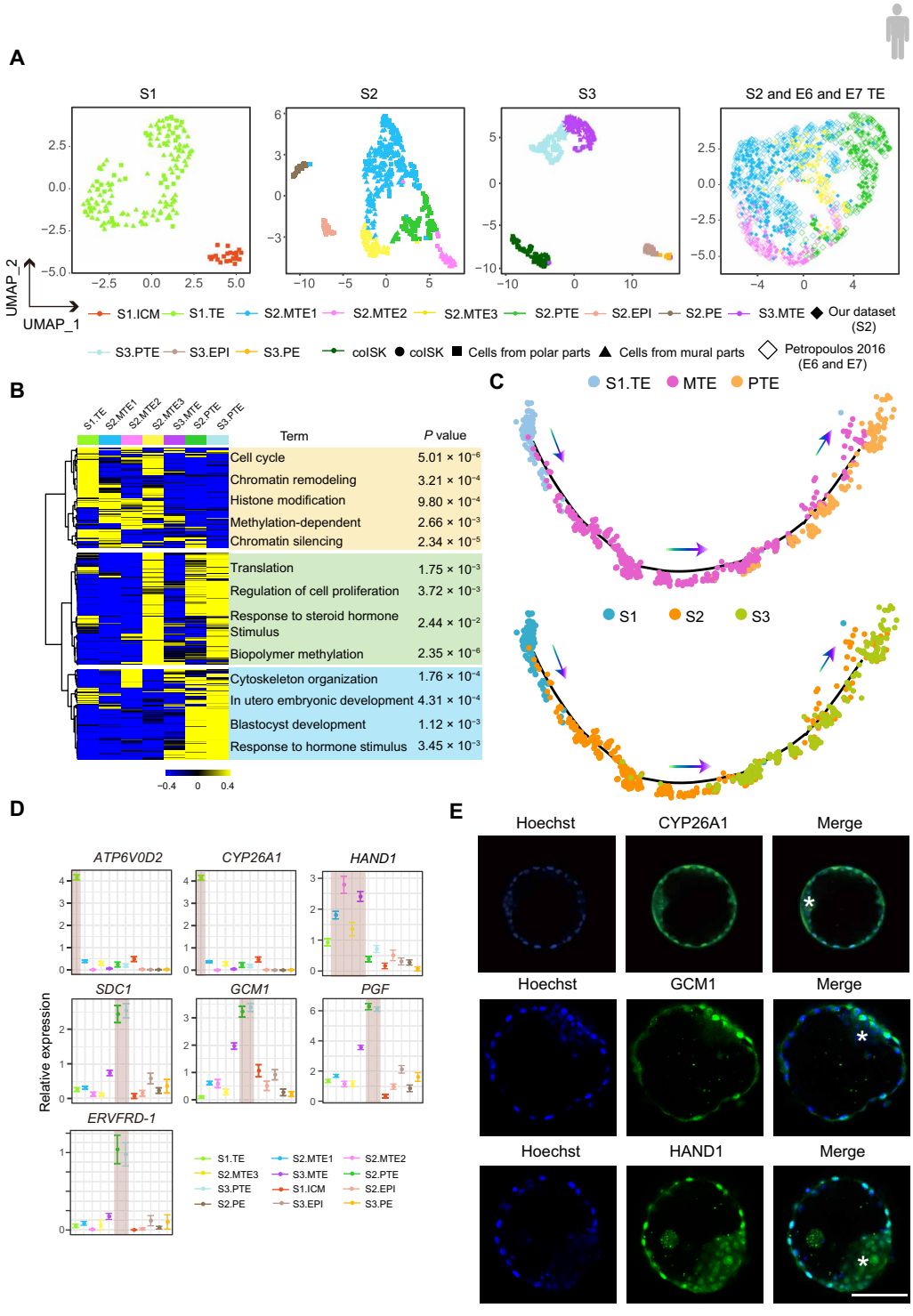

Fig. 2. Human TE cell differentiation during peri-implantation. (**A**) Cell lineage identification of S1, S2, and S3 TEs (first three columns). Integrated analysis of S2 TE in this study and E6 and E7 TE from the previous study [Petropoulos *et al.* (*5*)] (last column). (**B**) Unsupervised hierarchical clustering of highly variable genes in TE cells of three stages and the corresponding GO analysis. (**C**) Pseudotime analysis of TE cells of three stages. The arrows show the developmental trajectory. Colors represent corresponding cell types. (**D**) Dot plots show relative gene expression levels [$\log_2$ (TPM/10 + 1), average levels ± SEMs] of specifically expressed genes for each TE cell type. (**E**) Immunofluorescence images of the TE-specific gene CYP26A1 in S1 embryos, MTE-specific gene HAND1, and the PTE-specific gene GCM1 in S2 embryos. ICM is marked by an *. Scale bar, 100 μm.

penetration into the endometrium by the polar face. Other genes mentioned by Petropoulos *et al*. (*5*) to be highly expressed in PTE (including *CCR7*, *CYP19A1*, *DLX5*, and *MUC15*) (*5*) were confirmed to be expressed in the PTE in this study (fig. S3C).

TE cell differentiation in mice

Mouse embryos implant with the MTE (distant from the ICM), in contrast to human embryos (fig. S6A). To compare TE cell development between humans and mice, we performed scRNA profiling of mouse embryos at stages corresponding to that we examined in humans. In total, 592 cells from 26 mouse embryos were analyzed (figs. S1A and S6, B and C; and table S4). Similar to human embryos, mouse TE cells initiated their differentiation at S2 after hatching from the zona. However, mouse PTE cells were not clearly identifiable until S3 (Fig. 3A). In mice, as in humans, PTE cells were more mature than MTE cells (fig. S6D). Previously identified genes that regulated trophoblast development, such as *Gata3* (*33*) and *Rxra* (*24*), were preferentially expressed in mouse MTE cells (Fig. 3B). MTE cells were more active than PTE cells in actin filament–based cytoskeleton activities and cell adhesion, which are required for mural TE cells to phagocytize and penetrate the luminal epithelium (fig. S6E and table S5) (*34*).

In human embryos, the TE cells at the implantation pole were more quiescent than those at the opposite pole; a similar finding was observed in mouse embryos, with the implantation pole being the MTE instead of the PTE (Fig. 3C and fig. S4B). In humans, Ki67 immunostaining showed a higher proliferation capacity in the MTE than in the PTE, while the opposite was true in mice (Fig. 3D). On the other hand, both human PTE and mouse MTE expressed genes related to placental development, with their expression profiles being species specific. For example, as expected, the mouse trophoblast stem cell markers *Eomes* and *Elf5* (*28*, *35*, *36*) were highly expressed in mouse TE but rarely detected in human embryos. On the other hand, *OVOL1* and *CGA*, two genes related to trophoblast syncytialization and hormone production (*37*), were expressed exclusively in human trophoblasts (Fig. 3E). The implantation poles of both species (PTE in humans and MTE in mice) shared 34 and 9 DEGs in S2 and S3 embryos, respectively (fig. S6F and tables S6 and S7). These genes are involved in various cellular processes during implantation, such as cell recognition and adhesion (*B3GNT5* and *TIANL1*) (*38*, *39*), cell migration (*LCP1*, *EFHD2*, and *FMNL2*) (*40*–*42*), immune tolerance (*CSF3R*) (*43*), placentation and cell lineage specification (*RXRA*, *GATA2/3*, *TFAP2AC*, and *ARID3A*) (*33*), and hormone stimuli (*TEAD3*) (*44*). In addition, the AKT/PI3K (phosphatidylinositol 3-kinase)/mTOR (mammalian target of rapamycin) pathway, which participates in metabolism, cell growth, the immune response, and the DNA damage response (*45*), was observed among the common DEGs of implantation poles (Fig. 3, F and G). Of these genes, the formin *FMNL2* was colocalized with actin filaments at the attachment site (Fig. 3H). However, the PTEs from humans and mice showed few similarities. Overall, both human and mouse PTEs were more mature than MTEs. Accordingly, some of the genes participating in implantation and placentation were conserved in the implantation poles of these two species.

We further used SCENIC (Single-Cell rEgulatory Network Inference and Clustering) to predict some potential transcription factors for each cell type at each stage in both humans and mice (fig. S7). Consistently, many transcription factors related to trophoblast development, such as *ESRRB*, *CDX2*, and *TEAD4*, were enriched TE cells. *GATA3*, *RXRA*, *ARID3A*, and *BHLHE40* showed a high transcriptional activity at the implantation poles in both humans and mice. These results demonstrate the importance of these genes for embryo implantation and conservation between species.

Embryo–endometrial cell interaction during attachment

The molecular mechanisms underlying cell-cell communication between the TE and endometrium during implantation remain unclear. To better understand this process, we used an embryo–ISK cell coculture system to mimic in utero embryo implantation. Analysis results showed that among the genes encoding adhesion molecules, including mucins (MUCs), galectins (LGALSs), integrins (ITGA and ITGB), and extracellular matrix (ECM) molecules, the genes *MUC15*, *LGALS3*, and *ITGA5* were enriched in S2 PTE and S3 PTE, and *MUC1*, *LGALS1*, *LGALS8*, *ITGAV*, *ITGA3*, *ITGA5*, *ITGA6*, *ITGB4*, and *ECM1* were enriched in coISK cells (Fig. 4A). We also used CellPhoneDB (*46*) to predict cell-cell interactions between coISK and S3 PTE. Multiple desmocollins (*DSC1*, *DSC2*, and *DSC3*) and a desmoglein (*DSG2*) were enriched in polar TE cells and coISK cells, respectively, indicating that there was a close mediation of cell-cell junctions between the embryos and the endometrium. Furthermore, several gene pairs mediating cell-cell interactions (i.e., ligands and receptors) were also enriched in S3 PTE and coISK, including *CCL5-ACKR2*, *CD274-PDCD1*, *APP-CD74*, and *FLT1-VEGFA*; these gene pairs are presumably involved in the inflammatory response (*47*), fetomaternal tolerance (*48*, *49*), and early angiogenesis (*50*) during implantation (Fig. 4, B and C; fig. S8E; and table S8). The interactions between ICM and TE cells at each developmental stage in humans and mice were also explored. The expression levels of *CCL5-CCR1* and *CCL5-ACKR2* [responsible for the recruitment of effector immune cells (*51*, *52*)] increased during human embryonic development, indicating that EPI might regulate PTE in immune responses at the maternal-fetal interface. In mice, TE cells exhibited more active regulation of EPI development (fig. S8, A to D). To explore the effects of the embryo on the development of endometrial cells, ISK cells either cocultured with an embryo or grown without an embryo (*53*) were analyzed (Fig. 4D and table S9). Genes related to cell proliferation, retinoic acid signaling, and embryo attachment were up-regulated in coISK cells, including *TMAB4X*, *SLC7A8*, *RGCC*, *FABP5*, and *ATF3* (Fig. 4E).

Embryo implantation failure

In addition to the five successfully attached (AS) S3 embryos (E15 to E18 and E23), four (E26 to E29) failed to attach to ISK cells and were defined as "AF" (attachment failure) embryos (Fig. 5A and table S10). The TE cells in these AF embryos expressed similar subtype-specific genes with AS embryos (fig. S9A). To exclude possible biases caused by individual differences, we individually analyzed each AF MTE. The gene expression patterns of MTE cells in AF embryos were substantially different from those in attached embryos; however, the gene expression patterns of PTE cells were similar between the two types of embryos (Fig. 5B). GO analysis of the overlapping DEGs in MTE and PTE cells in AF embryos showed up-regulation of genes regulating translational elongation, such as *RPS28*, *RPS29*, *RPS12*, and *RPL17* (Fig. 5, C to E, and fig. S9, B and F). *TPT1*, which plays a role in the response to DNA damage (*54*), was also up-regulated in AF embryos (Fig. 5E). Proteasome subunits that regulate ubiquitin protein ligase activity were down-regulated in AF embryo MTE cells. Genes encoding mitochondrial ribosomal

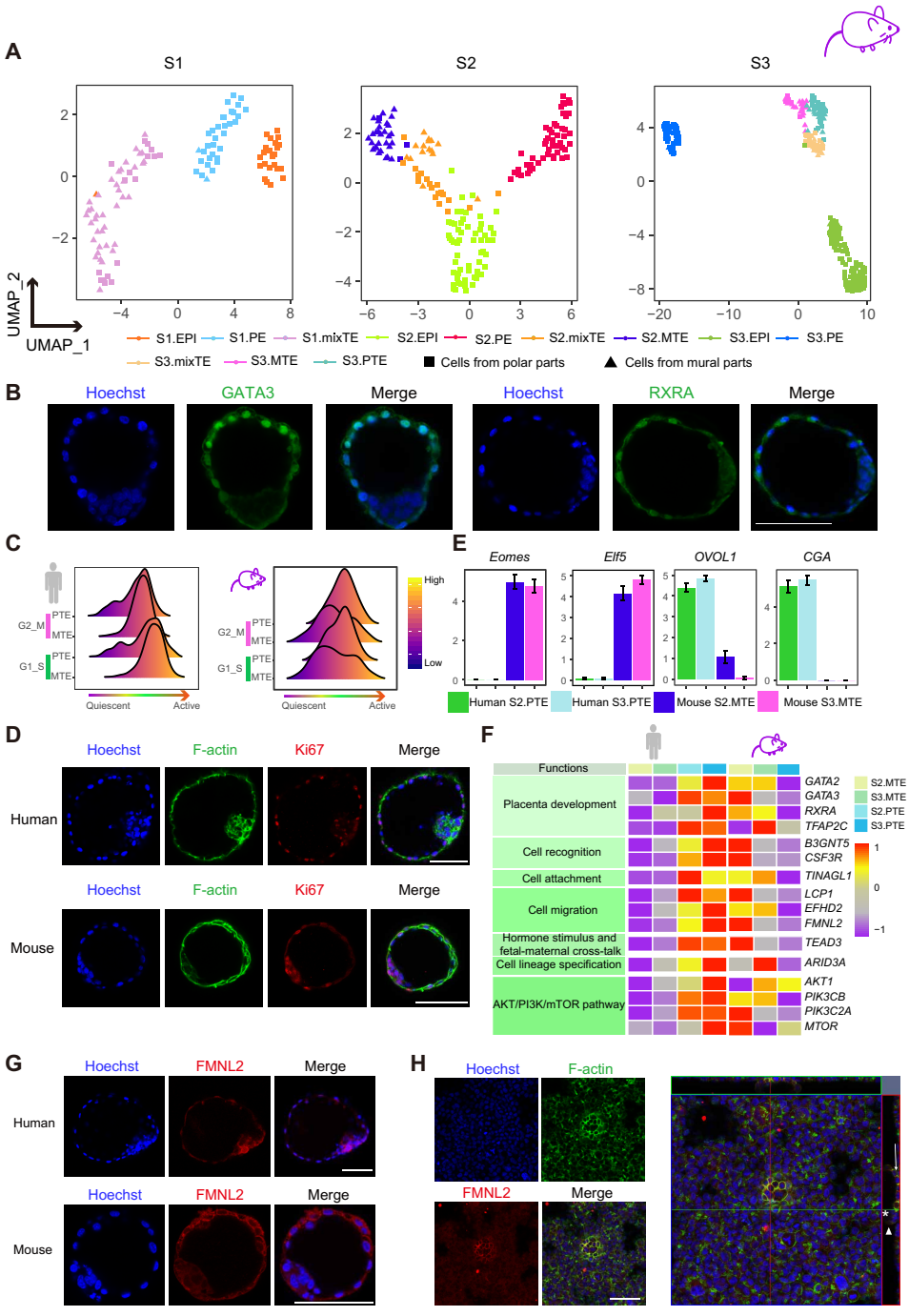

Fig. 3. Comparison of mouse TE with human TE. (**A**) Cell lineage identification of mouse S1, S2, and S3 TEs. (**B**) Immunofluorescence images of GATA3 and RXRA in mouse S2 embryos. Scale bar, 100 μm. (**C**) Cell cycle analysis of MTE and PTE in human and mouse. (**D**) Immunofluorescence images of Ki67 in human and mouse S2 embryos. Scale bars, 100 μm. (**E**) Bar plots showing relative expression levels [$\log_2$ (TPM/10 + 1), average levels ± SEMs] of specific genes in the implantation pole of human and mouse embryo. (**F**) Expression pattern and functional annotations of the common DEGs in implantation poles of human and mouse embryo. (**G**) Immunofluorescence images of FMNL2 in human and mouse S2 embryos. (**H**) The left panel shows immunofluorescence images showing colocalization of Fmnl2 and F-actin at the attachment site of mouse embryos. The right panel shows the same image with top view and side view. Please note that in the side view, ICM is marked by an *, MTE is marked by an arrow, and PTE is marked by an arrowhead. Scale bar, 100 μm.

proteins, mitochondrial organization proteins (such as *TIMM50*, *TIMM23*, and *TIMMDC1*), and NADH (reduced nicotinamide adenine dinucleotide)–ubiquinone oxidoreductase subunits were markedly down-regulated in the MTE of AF embryos (Fig. 5, D to F). The overall TE in AF embryos showed a similar expression pattern of decreased ubiquitin protein ligase activity and energy production compared to the three TE stages in AS embryos (fig. S9C). The expression level of eukaryotic initiation factor 6 (*EIF6*), which has

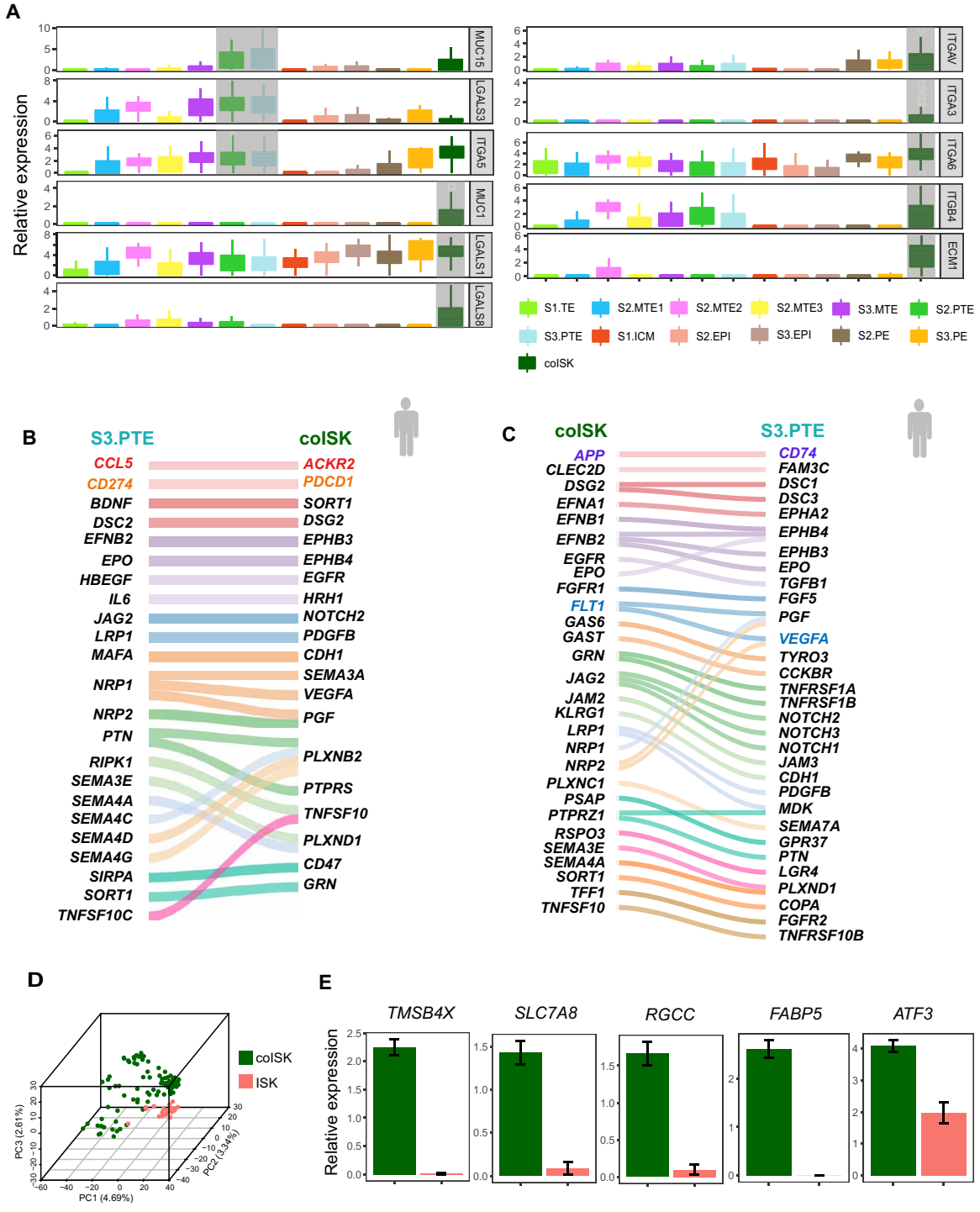

Fig. 4. Embryo–endometrial cell interactions during attachment. (**A**) Cell adhesion molecule enrichment analysis in embryo cells and colSK cells. Relative expression levels are defined as $\log_2$ (TPM/10 + 1). (**B** and **C**) Top ligand-receptor pairs predicted by CellPhoneDB between colSK and S3PTE. (**D**) Three-dimensional PCA plot of DEGs between cocultured ISK cells (colSK) and control ISK cells. (**E**) Bar plots showing relative expression levels [$\log_2$ (TPM/10 + 1), average levels ± SEMs] of selected genes induced in colSK.

been reported to control cell motility, invasiveness (*55*), and proliferation (*56*), also decreased, suggesting impaired cell motion and proliferation in the MTE of unattached embryos (Fig. 5E). The methyltransferase *METTL5* [an enzyme responsible for 18S ribosomal RNA (rRNA) m^6A methylation] and its activator *TRMT112* were down-regulated in AF embryo MTE cells, while the demethylase *ALKBH5* was up-regulated in three of the four unattached embryos (Fig. 5E and fig. S9F). Knockout of *Trmt112* by CRISPR-Cas9 in mouse zygotes did not affect the blastocyst formation rate (fig. S9G). However, none of the *Trmt112* knockout (KO) embryos resulted in

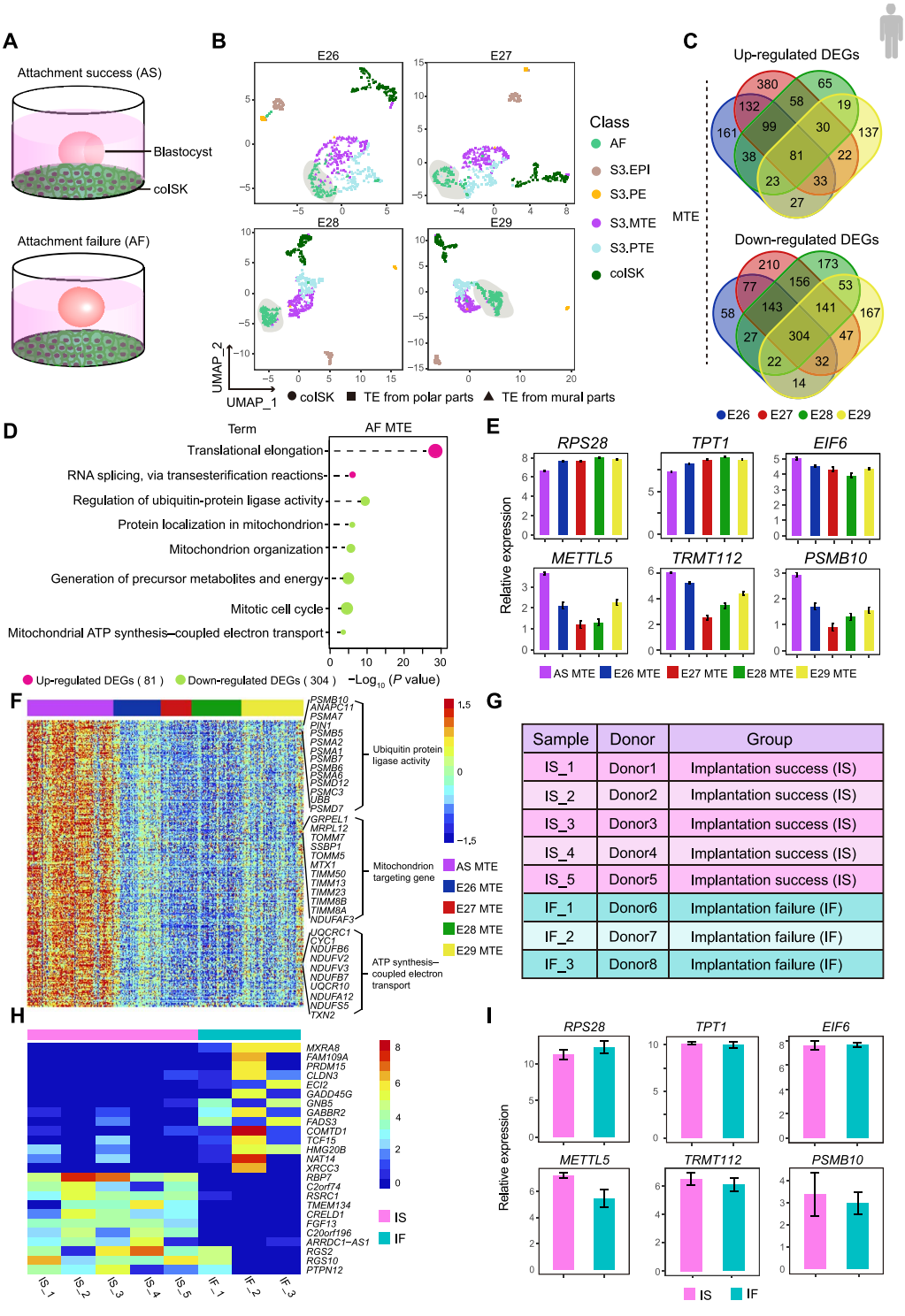

Sample	Donor	Group
IS_1	Donor1	Implantation success (IS)
IS_2	Donor2	Implantation success (IS)
IS_3	Donor3	Implantation success (IS)
IS_4	Donor4	Implantation success (IS)
IS_5	Donor5	Implantation success (IS)
IF_1	Donor6	Implantation failure (IF)
IF_2	Donor7	Implantation failure (IF)
IF_3	Donor8	Implantation failure (IF)

Fig. 5. Analysis of embryos that failed to attach in vitro or failed to implant in the clinic. (**A**) Schematic of the embryo–ISK cell coculture model. Top: AS. Bottom: AF. (**B**) UMAP analysis of each AF embryo and AS embryos. (**C**) The number of up- and down-regulated DEGs in four AF embryos. (**D**) GO analysis of overlapped up- and down-regulated DEGs in the AF embryos. The circle sizes display the number of involved genes in each term. (**E**) Bar plots showing relative expression levels [$\log_2$ (TPM/10 + 1)] of selected up- and down-regulated genes in the AS and AF MTE. (**F**) Heatmap shows the expression levels of DEGs between AS and AF MTE. Colors from blue to red represent the expression level from low to high. (**G**) Sample information of embryos with successful or failed implantation embryos in PGT. (**H**) Heatmap showing the expression levels of DEGs between IS and IF (implantation failure) embryos. Colors from blue to red indicate the expression level from low to high. (**I**) Bar plots showing relative expression levels [$\log_2$ (TPM/10 + 1)] of representative genes in IS and IF MTE.

a live birth (fig. S9H). When *Trmt112* was specifically knocked down in trophoblast cells by lentivirus-mediated RNA interference, the embryo attachment rate was significantly reduced (fig. S9I). These results indicate that reduced 18*S* rRNA m^6A methylation activity in MTE cells might affect embryo attachment to the endometrium.

Preimplantation genetic testing (PGT) is widely used in assisted reproductive technology (ART) to prevent birth defects and genetic diseases by identifying defects before gestation. During the PGT procedure, a cluster of cells is biopsied, including 5 to 10 TE cells from the mural part of a blastocyst, for genetic analysis. In this study, one or two cells from the same biopsied cluster were isolated for transcriptome sequencing to identify key genes that might regulate embryo implantation. Embryos that had normal chromosomes and were free of known single-gene disorders were transferred after genetic diagnosis. The clinical outcomes of eight PGT embryos transferred from January 2016 to August 2016 were followed up. Among these eight embryos, five implanted successfully (IS), leading to delivered babies, and the other three underwent implantation failure (Fig. 5G, fig. S9D, and table S10). Similar to our in vitro results concerning the up-regulation of translational elongation genes (such as *RPS28* and *RPS29*) in AF MTE, these two genes were also up-regulated in IF biopsies (Fig. 5I and fig. S9, E and F). In addition, genes involved in protein metabolism, mitochondrion organization, and 18*S* rRNA m^6A methylation as well as genes involved in implantation (*FGF13* and *RBP7*) and DNA repair (*C20orf196*, also known as *SHLD1*) were down-regulated in cells from IF embryos (Fig. 5, H and I, and fig. S9, E and F). Overall, the MTE cells of IF and AF embryos displayed similar malfunctions in protein metabolism, 18*S* rRNA m^6A methylation, and energy production.

DISCUSSION

At the blastocyst stage, the ICM is surrounded by the TE, a single layer of epithelial cells that directly contacts the endothelium and later transforms to a vital organ transporting oxygen and nutrition to the fetus. Our data characterized two peri-implantation–stage TE subpopulations, derived from polar and mural poles, and assessed their correlations with embryo implantation. In our methods, instead of digesting the whole blastocyst (*5*, *6*), we collected single cells following physical dissection of the embryo into two parts along the edge of the ICM. The definition of the TE cell subpopulation in this study was consistent with that in previous studies. Our data showed that the TEs from the two sides were transcriptionally similar before hatching (with an intact zona pellucida). Meistermann *et al.* (*6*) reported that TE differentiation originated at the stages of expanded/hatched blastocysts, which is similar to our observation. In our study, *ESRRB* and *POU5F1* showed higher expression activity in S1 TE than in S2/3 TE. These results support the prior study on TE cell plasticity, in which reaggregated TE cells from early-stage human blastocysts were able to form a new blastocyst with an ICM (*22*). However, the plasticity of TE cells at different stages still needs to be carefully evaluated.

Beginning when the blastocysts hatched (or perhaps earlier, at the B5 stage), subpopulations of PTE and MTE were identified. The former population was more differentiated than the latter and expressed villous STB marker genes. However, unlike STB cells, with their irregular shapes and conspicuously large size, TE cells from the polar side in our study were regular in shape and average in size. In addition, at the attachment stage, PTE is less syncytialized and less migratory than the subsequent day 8 STB (*18*). Multinucleated cells can be formed either by cell-cell fusion or by endoreplication. Blastocyst PTE expressed fusion genes such as *ERVFRD-1* (Syncytin-2), *GCM1*, and *OVOL1*. We also observed that endoreplication-related genes were up-regulated (*CCNE1*/*CDK2*) or down-regulated (*CCNB1*/*CDK1*) in S3 TE compared with earlier-stage TE (*57*). The villous STB is formed by the fusion of cytotrophoblasts (CTBs) (*19*). These results imply that the formation of primitive multinucleated cells at the beginning of implantation may be established in a different manner. However, follow-up studies that include protein quantification and functional experiments are required for further validation. MTE shows higher proliferative activity than PTE; thus, the TE cell replenishment would be more reliant upon MTE. Villous CTB acts in a similar way to replenish STB and extravillous trophoblast. However, MTE does not consistently express villous CTB marker genes (*19*) or early-stage CTB marker genes (*18*, *20*). The roadmap from blastocyst TE to placental trophoblast could be more complicated.

Mouse models have long been used as powerful tools to study human embryo implantation. However, the fact that human and mouse embryos attach to the endometrium in opposite directions has led to the issue that some of the mechanisms found in mice are not identical to those in humans (*8*). A comparative study of human and mouse TE specification might further expand our understanding of which mechanisms are shared or not shared between humans and mice. Some implantation- and placentation-related genes are conserved at the implantation poles in humans and mice. Specifically, *FMNL2*, which facilitates F-actin assembly to form lamellipodial protrusions (*42*), was enriched at the implantation poles of both humans and mice. These lamellipodial protrusions could be vital for the interactions between the embryo and endometrium at the apposition stage, which ultimately guide the embryo attachment in the right direction. On the other hand, the TEs of the nonimplantation poles in humans (MTE) and mice (PTE) are more active in cell proliferation and energy production, which are necessary for TE development.

Human TE-endometrium interaction at the beginning of implantation is poorly understood because of the inaccessibility of the materials in vivo. The coculture system using embryos and endometrial cells makes it possible to investigate cell-cell cross-talk at the attachment site. Here, we used a simple coculture system using an adenocarcinoma-derived endothelial cell line (ISK cells), whose cell characteristics are easy to sustain. Notch signaling, critical for fetal-maternal communication during implantation and placentation (*58*), was enriched in our analysis. Recently, researchers from Austria found that the gene pair *PGF-NRP1* was highly enriched in the polar TE of derived blastoid and endometrial organoid cells (*59*), and this finding was consistent with our results. To some extent, this model can recapitulate the cell-cell interactions that occur in vivo. However, it is important to mention that the attachment surface of ISK cells does not exactly mimic that of uterine endometrial epithelial cells, as ISK cell line is immortal.

Because embryo implantation is a complex process involving multiple factors, any of a variety of fetal or maternal abnormalities can result in implantation failure. To address this issue, we investigated the altered gene expression of embryos that failed to attach in vitro or implant in vivo. PGT is a powerful tool that allows us to examine the genomic integrity and gene expression patterns of a few mural TE cells obtained from embryos before uterine transfer. MTE cells collected from embryos that either failed to implant

clinically or failed to attach in our in vitro coculture system exhibited similar transcriptional characteristics, including abnormalities in mitochondrial gene expression and protein metabolism, decreased 18*S* rRNA m^6A methyltransferase activity, and increased demethylase activity. It has been reported that m^6A modification in rRNA is important in programs such as stemness, differentiation, and development (*60*). In placental trophoblasts obtained from patients with recurrent miscarriages, the global levels of mRNA m^6A methylation are significantly decreased, while those of the m^6A demethylase *ALKBH5* are increased (*61*). Therefore, these disorders in MTE cells could be regarded as potential embryonic causes that affect the implantation process. In clinical practice, human embryo quality is conventionally determined through morphological evaluation by skilled embryologists (manual grading). All the embryos that were seeded onto ISK cells or transferred into the uterus after PGT were highly qualified for transfer. As shown in our results, morphologically sound embryos did not necessarily result in successful implantation. Recent studies showed that the ratio of mitochondrial DNA (mtDNA) to genomic DNA (gDNA), i.e., mtDNA/*gDNA*, could be used to predict blastocyst development (*62*). On the basis of these studies, our novel findings may yield useful indicators to help assess embryo quality for transfer during ART.

In summary, we provided a time-course analysis of TE cell specification during implantation. In addition, we described the gene expression characteristics of different TE subpopulations in both human and mouse embryos. Moreover, we discussed the cross-talk between the embryo and endometrium and the possible factors that may lead to implantation failure. Therefore, this study provides valuable information and future directions for embryo implantation research, which might potentially benefit patients with recurrent implantation failure.

MATERIALS AND METHODS

Human embryo preparation

Embryos were obtained from couples undergoing standard clinical IVF protocols at the Center for Reproductive Medicine of Peking University Third Hospital. The average age of the women was 30 years (25 to 35 years).

Embryo–ISK cell coculture system

The embryo–ISK cell coculture system has been described previously (*13*). Briefly, the ISK cell line (a gift from the laboratory of H. Wang) was maintained in phenol red–free DMEM/F-12 medium (11039, Gibco) supplemented with 10% charcoal-stripped fetal bovine serum (CFBS) and penicillin-streptomycin. The day before coculture, ISK cells were passaged to a glass-bottom dish. Fully hatched embryos were seeded onto the cell surface at 70 to 80% confluence in DMEM/F-12 medium supplemented with 30% CFBS, progesterone (63.5 nM), estradiol-17β (7.14 nM), epidermal growth factor (20 ng/ml), and penicillin-streptomycin. The dish was placed in a CO_2 incubator for 24 hours before the following steps.

Separation of PTE and MTE by embryo microdissection

Embryos were cut with a laser along the edge of the ICM until the polar side, and the mural side was completely separated into two masses under the micromanipulator. These two masses of cells were incubated in digestion solution containing Accutase/trypsin (1:1) for 30 min until most of the cell mass had dissociated into single cells. The mural cell mass contained the MTE, while the polar cell mass contained the PTE as well as the ICM. Inner cells were excised according to marker gene expression by scRNA-seq analysis.

Mouse embryo preparation

Eight- to 10-week-old female $B6D2F_1$ mice were superovulated to obtain mature oocytes as described previously (*63*); they were then mated with 129S2/Sv male mice to collect embryos. The blastocysts were obtained from the uterus at E3.5 (S1). Mouse embryos were cultured with KSOM medium (MR-020P-F, Millipore) at 37°C and 5% CO_2 until they hatched from the zona (S2). The hatched embryos were cocultured with ISK cells for 24 hours (S3). The capture of single cells from the mural and polar sides was performed in the same way as in the human embryos.

Immunofluorescence

The embryos were fixed with 4% paraformaldehyde in DPBS (Dulbecco's Phosphate-Buffered Saline) for 30 min at room temperature and then washed three times with 0.1% human serum albumin (HSA) in DPBS. Then, 1% Triton X-100 was applied for 30 min at room temperature for membrane permeabilization. The embryos were washed and then blocked with 3% bovine serum albumin in DPBS at room temperature for 90 min. Next, the embryos were incubated with primary antibodies [glial cells missing transcription factor 1 (GCM1) antibody, NBP2-48520, Novus; heart and neural crest derivatives expressed 1 (HAND1) antibody, ab196622, Abcam; CYP26A1, sc-53618, Santa Cruz Biotechnology; PGF antibody, ab9542, Abcam; OCT3/4 (octamer-binding protein 3/4, also called POU class 5 homeobox 1) antibody, sc-5279, Santa Cruz Biotechnology; OCT4 antibody, ab19857, Abcam; FMNL2 (formin like 2) antibody, sc-390298, Santa Cruz Biotechnology; GATA3 (GATA binding protein 3) antibody, ab199428, Abcam; RXRA (retinoid X receptor alpha) antibody, ab125001, Abcam; and Ki67 antibody, ab15580, Abcam] at 4°C overnight. The embryos were washed with washing solution (DPBS with 0.1% Tween 20 and 0.01% Triton X-100) three times for 5 min each and then incubated with secondary antibodies [goat anti-rabbit immunoglobulin G (IgG) Alexa Fluor 488, A11008, Invitrogen; goat anti-mouse IgG Alexa Fluor 488, A11001, Invitrogen; goat anti-mouse IgG Alexa Fluor 555, A21422, Invitrogen; and TRITC, goat anti-rabbit IgG, ZF-0316, ZSGB-BIO] in blocking solution for 1 hour at room temperature. After being washed, the samples were stained with Hoechst 33342. The samples were imaged with confocal microscopy (Carl Zeiss 710), and the images were processed with ZEN imaging software (Carl Zeiss).

scRNA-seq library construction and sequencing

Single cells were captured with a mouth pipette and washed in DPBS with 0.1% HSA. Then, the cells were transferred to lysis buffer. Single-cell transcriptome libraries were constructed with a modified single cell–tagged reverse-transcription sequencing method (*64*). Briefly, the single cells were lysed to release the RNA. We reverse-transcribed the RNA using oligo(dT) primers with cell-specific barcodes and unique molecular identifier (UMI) sequences. The complementary DNA (cDNA) was amplified via 18 cycles of PCR. Next, the single-cell amplification products were pooled together and purified. Subsequently, the cDNA was used as a template for four cycles of PCR with an IS primer and a biotin index primer to add biotin modification at the 3′ ends of the cDNA strands. Then, 300 ng of cDNA was fragmented into lengths of approximately 300 base pairs (bp) with Covaris M220. We used Dynabeads MyOne

Streptavidin C1 beads (65001, Thermo Fisher Scientific) to enrich the 3′ terminal cDNAs and then constructed a sequencing library with the Kapa HyperPrep Kit (KK8504, Kapa Biosystems). At least 1 Gb of sequencing data for each individual cell was generated on the Illumina HiSeq 4000 platform with 150-bp paired-end sequencing.

Processing of scRNA-seq data

First, the raw paired-end reads were separated with the help of the distinct cell barcode information in read 2. Second, according to the ReadID information, the corresponding read 1 was obtained. Third, we trimmed the template-switch oligonucleotide sequence, poly(A) tail sequence, low-quality bases ($N > 10\%$), and adaptor contamination from read 1. Next, using TopHat (v2.0.12) (*65*), we aligned the processed reads to the hg19 human reference genome [UCSC (University of California Santa Cruz)]. Subsequently, using the HTSeq package (*66*), we counted and grouped the uniquely mapped reads. For each gene, we removed duplicated transcripts based on the UMI information. Last, for each unique UMI, we quantified the transcript copy number and used $\log_2$ (TPM/10 + 1) for downstream analysis, where TPM is the number of transcripts per million. For the human data, we set the filter criteria as follows: The number of expressed genes in each cell was more than 2000 genes, and the number of transcripts was more than 10,000. For the mouse data, we set the primary filter criteria as follows: The number of expressed genes in each cell was more than 1200 genes, and the number of transcripts was more than 10,000. In addition, the second maximum pairwise and Pearson correlations were required to be greater than 0.6 (*5*).

Cell cluster identification

The R package Seurat was applied to perform cell cluster classification on the normalized TPM expression values of the filtered data (*67*). Highly variable genes were selected using the "FindVariableGenes" function and used as input for a PCA. Jackstraw analysis with 100 replicates was used to select principal components (PCs) that could significantly separate the cells (*68*). After that, the significant PCs were used to perform UMAP analysis through the RunUMAP function.

Identification of DEGs within each cluster

The FindMarkers function (test.use = "roc") of the Seurat package was applied to the normalized TPM expression values to identify distinct cluster-specific marker genes with power > 0.4. GO analysis was performed using The Database for Annotation, Visualization and Integrated Discovery (DAVID) (https://david.ncifcrf.gov/tools.jsp).

Cell cycle analysis

In total, 43 G_1-S and 54 G_2-M cell cycle–related genes were used as input for cell cycle analysis (*69*, *70*).

Construction of single-cell trajectories for TE clusters

Monocle v2.6.4 (*71*) was applied to construct the trajectory landscape of TE development. Tendency plots were plotted using the ggplot2 package in pseudotime order.

Reclassification of DEGs from three human TE clusters by developmental time

We applied an R package (cummeRbund) to group the DEGs from three human TE cluster cells in pseudotime order using genesCluster ($k = 9$).

Cell-cell interaction analysis

CellPhoneDB software was used to integrate a database, consisting of ligands, receptors, and interaction modules, to systematically predict cell-cell interactions using the default parameters (https://github.com/Teichlab/cellphonedb) (*46*). For the top interaction pairs, we applied the R package scmap to visualize the interaction modules.

CRISPR-Cas9–mediated knockout in mouse zygotes

Trmt112 single guide RNAs (sgRNAs) (sgRNA1, GGGGTTGATGCGGACCTCAG; and sgRNA2, TGCAGGCAGCGGACACCGTA) and spCas9 proteins were electrotransfected into mouse zygotes (performed by JiShiJinBian, Beijing, China). Zygotes were cultured for further experiments.

Trophoblast-specific knockdown by a lentiviral vector

Trmt112 short hairpin RNAs (shRNAs) (sequence 1: 5′-GAAACTGCTCACCCACAATCT-3′; sequence 2: 5′-GCTGTTGAATGATGAGGAGAC-3′; sequence 3: 5′-ACCCTGCAATGCCCAGAATCT-3′) and scramble control shRNA (5′-TTCTCCGAACGTGTCACGT-3′) were subcloned into the pGLV3/H1/green fluorescent protein lentiviral vector (GenePharma, Shanghai, China). The lentivirus was diluted in embryo culture medium to 8×10^6 TU (transducing units)/ml with polybrene (5 μg/ml). The zona was removed from each mouse blastocyst before individual incubation in 15 μl of diluted lentivirus droplets for 4 hours. Then, the embryos were cocultured with ISK cells as described above.

SUPPLEMENTARY MATERIALS

Supplementary material for this article is available at https://science.org/doi/10.1126/sciadv.abj3725

View/request a protocol for this paper from *Bio-protocol*.

REFERENCES AND NOTES

1. G. Haddad, M. Deng, C. T. Wang, C. Witz, D. Williams, J. Griffith, J. Skorupski, J. Gill, W. H. Wang, Assessment of aneuploidy formation in human blastocysts resulting from donated eggs and the necessity of the embryos for aneuploidy screening. *J. Assist. Reprod. Genet.* **32**, 999–1006 (2015).
2. B. C. Paria, Y. M. Huet-Hudson, S. K. Dey, Blastocyst's state of activity determines the "window" of implantation in the receptive mouse uterus. *Proc. Natl. Acad. Sci. U.S.A.* **90**, 10159–10162 (1993).
3. S. Moustafa, S. L. Young, Diagnostic and therapeutic options in recurrent implantation failure. *F1000Res* **9**, F1000 Faculty Rev-208 (2020).
4. D. Vinatier, J. C. Monnier, The fetal-maternal interface. Description of its elements from an immunologic perspective. *J. Gynecol. Obstet. Biol. Reprod.* **19**, 691–700 (1990).
5. S. Petropoulos, D. Edsgard, B. Reinius, Q. Deng, S. P. Panula, S. Codeluppi, A. Plaza Reyes, S. Linnarsson, R. Sandberg, F. Lanner, Single-cell RNA-seq reveals lineage and X chromosome dynamics in human preimplantation embryos. *Cell* **165**, 1012–1026 (2016).
6. D. Meistermann, A. Bruneau, S. Loubersac, A. Reignier, J. Firmin, V. Francois-Campion, S. Kilens, Y. Lelievre, J. Lammers, M. Feyeux, P. Hulin, S. Nedellec, B. Bretin, G. Castel, N. Allegre, S. Covin, A. Bihouee, M. Soumillon, T. Mikkelsen, P. Barriere, C. Chazaud, J. Chappell, V. Pasque, J. Bourdon, T. Freour, L. David, Integrated pseudotime analysis of human pre-implantation embryo single-cell transcriptomes reveals the dynamics of lineage specification. *Cell Stem Cell* **28**, 1625–1640.e6 (2021).
7. K. Y. Lee, F. J. DeMayo, Animal models of implantation. *Reproduction* **128**, 679–695 (2004).
8. H. Wang, S. K. Dey, Roadmap to embryo implantation: Clues from mouse models. *Nat. Rev. Genet.* **7**, 185–199 (2006).
9. J. L. James, A. M. Carter, L. W. Chamley, Human placentation from nidation to 5 weeks of gestation. Part I: What do we know about formative placental development following implantation? *Placenta* **33**, 327–334 (2012).
10. A. T. Hertig, J. Rock, E. C. Adams, A description of 34 human ova within the first 17 days of development. *Am. J. Anat.* **98**, 435–493 (1956).
11. M. N. Shahbazi, A. Jedrusik, S. Vuoristo, G. Recher, A. Hupalowska, V. Bolton, N. N. M. Fogarty, A. Campbell, L. Devito, D. Ilic, Y. Khalaf, K. K. Niakan, S. Fishel,

M. Zernicka-Goetz, Self-organization of the human embryo in the absence of maternal tissues. *Nat. Cell Biol.* **18**, 700–708 (2016).
12. F. Zhou, R. Wang, P. Yuan, Y. Ren, Y. Mao, R. Li, Y. Lian, J. Li, L. Wen, L. Yan, J. Qiao, F. Tang, Reconstituting the transcriptome and DNA methylome landscapes of human implantation. *Nature* **572**, 660–664 (2019).
13. D. Zhang, P. Lv, R. Zhang, Q. Luo, G. Ding, L. Yin, J. Li, G. Xu, F. Qu, J. Sheng, H. Huang, A new model for embryo implantation: Coculture of blastocysts and Ishikawa cells. *Gynecol. Endocrinol.* **28**, 288–292 (2012).
14. A. Aberkane, W. Essahib, C. Spits, C. De Paepe, K. Sermon, T. Adriaenssens, S. Mackens, H. Tournaye, J. J. Brosens, H. Van de Velde, Expression of adhesion and extracellular matrix genes in human blastocysts upon attachment in a 2D co-culture system. *Mol. Hum. Reprod.* **24**, 375–387 (2018).
15. L. Yan, M. Yang, H. Guo, L. Yang, J. Wu, R. Li, P. Liu, Y. Lian, X. Zheng, J. Yan, J. Huang, M. Li, X. Wu, L. Wen, K. Lao, R. Li, J. Qiao, F. Tang, Single-cell RNA-Seq profiling of human preimplantation embryos and embryonic stem cells. *Nat. Struct. Mol. Biol.* **20**, 1131–1139 (2013).
16. P. Blakeley, N. M. Fogarty, I. del Valle, S. E. Wamaitha, T. X. Hu, K. Elder, P. Snell, L. Christie, P. Robson, K. K. Niakan, Defining the three cell lineages of the human blastocyst by single-cell RNA-seq. *Development* **142**, 3151–3165 (2015).
17. G. G. Stirparo, T. Boroviak, G. Guo, J. Nichols, A. Smith, P. Bertone, Integrated analysis of single-cell embryo data yields a unified transcriptome signature for the human pre-implantation epiblast. *Development* **145**, dev158501 (2018).
18. R. C. West, H. Ming, D. M. Logsdon, J. Sun, S. K. Rajput, R. A. Kile, W. B. Schoolcraft, R. M. Roberts, R. L. Krisher, Z. Jiang, Y. Yuan, Dynamics of trophoblast differentiation in peri-implantation-stage human embryos. *Proc. Natl. Acad. Sci. U.S.A.* **116**, 22635–22644 (2019).
19. Y. Liu, X. Fan, R. Wang, X. Lu, Y. L. Dang, H. Wang, H. Y. Lin, C. Zhu, H. Ge, J. C. Cross, H. Wang, Single-cell RNA-seq reveals the diversity of trophoblast subtypes and patterns of differentiation in the human placenta. *Cell Res.* **28**, 819–832 (2018).
20. L. Xiang, Y. Yin, Y. Zheng, Y. Ma, Y. Li, Z. Zhao, J. Guo, Z. Ai, Y. Niu, K. Duan, J. He, S. Ren, D. Wu, Y. Bai, Z. Shang, X. Dai, W. Ji, T. Li, A developmental landscape of 3D-cultured human pre-gastrulation embryos. *Nature* **577**, 537–542 (2020).
21. H. Gao, R. Gao, L. Zhang, W. Xiu, R. Zang, H. Wang, Y. Zhang, Y. Gao, J. Chen, S. Gao, Esrrb plays important roles in maintaining self-renewal of trophoblast stem cells (TSCs) and reprogramming somatic cells to induced TSCs. *J. Mol. Cell Biol.* **11**, 463–473 (2019).
22. C. De Paepe, G. Cauffman, A. Verloes, J. Sterckx, P. Devroey, H. Tournaye, I. Liebaers, H. Van de Velde, Human trophectoderm cells are not yet committed. *Hum. Reprod.* **28**, 740–749 (2013).
23. M. I. Morasso, A. Grinberg, G. Robinson, T. D. Sargent, K. A. Mahon, Placental failure in mice lacking the homeobox gene Dlx3. *Proc. Natl. Acad. Sci. U.S.A.* **96**, 162–167 (1999).
24. H. Huebner, A. Hartner, W. Rascher, R. R. Strick, S. Kehl, F. Heindl, D. L. Wachter, M. W. Beckmann Md, F. B. Fahlbusch, M. Ruebner, Expression and regulation of retinoic acid receptor responders in the human placenta. *Reprod. Sci.* **25**, 1357–1370 (2018).
25. Y. Barak, M. C. Nelson, E. S. Ong, Y. Z. Jones, P. Ruiz-Lozano, K. R. Chien, A. Koder, R. M. Evans, PPAR gamma is required for placental, cardiac, and adipose tissue development. *Mol. Cell* **4**, 585–595 (1999).
26. S. Langton, L. J. Gudas, CYP26A1 knockout embryonic stem cells exhibit reduced differentiation and growth arrest in response to retinoic acid. *Dev. Biol.* **315**, 331–354 (2008).
27. B. C. Han, H. F. Xia, J. Sun, Y. Yang, J. P. Peng, Retinoic acid-metabolizing enzyme cytochrome P450 26a1 (cyp26a1) is essential for implantation: Functional study of its role in early pregnancy. *J. Cell. Physiol.* **223**, 471–479 (2010).
28. T. K. Gamage, L. W. Chamley, J. L. James, Stem cell insights into human trophoblast lineage differentiation. *Hum. Reprod. Update* **23**, 77–103 (2016).
29. H. Okae, H. Toh, T. Sato, H. Hiura, S. Takahashi, K. Shirane, Y. Kabayama, M. Suyama, H. Sasaki, T. Arima, Derivation of human trophoblast stem cells. *Cell Stem Cell* **22**, 50–63.e6 (2018).
30. D. Baczyk, S. Drewlo, L. Proctor, C. Dunk, S. Lye, J. Kingdom, Glial cell missing-1 transcription factor is required for the differentiation of the human trophoblast. *Cell Death Differ.* **16**, 719–727 (2009).
31. J. Lu, S. Zhang, H. Nakano, D. G. Simmons, S. Wang, S. Kong, Q. Wang, L. Shen, Z. Tu, W. Wang, B. Wang, H. Wang, Y. Wang, J. H. van Es, H. Clevers, G. Leone, J. C. Cross, H. Wang, A positive feedback loop involving Gcm1 and Fzd5 directs chorionic branching morphogenesis in the placenta. *PLoS Biol.* **11**, e1001536 (2013).
32. M. Chang, D. Mukherjea, R. M. Gobble, K. A. Groesch, R. J. Torry, D. S. Torry, Glial cell missing 1 regulates placental growth factor (PGF) gene transcription in human trophoblast. *Biol. Reprod.* **78**, 841–851 (2008).
33. C. Krendl, D. Shaposhnikov, V. Rishko, C. Ori, C. Ziegenhain, S. Sass, L. Simon, N. S. Muller, T. Straub, K. E. Brooks, S. L. Chavez, W. Enard, F. J. Theis, M. Drukker, GATA2/3-TFAP2A/C transcription factor network couples human pluripotent stem cell differentiation to trophectoderm with repression of pluripotency. *Proc. Natl. Acad. Sci. U.S.A.* **114**, E9579–E9588 (2017).
34. D. D. Carson, I. Bagchi, S. K. Dey, A. C. Enders, A. T. Fazleabas, B. A. Lessey, K. Yoshinaga, Embryo implantation. *Dev. Biol.* **223**, 217–237 (2000).
35. A. P. Russ, S. Wattler, W. H. Colledge, S. A. Aparicio, M. B. Carlton, J. J. Pearce, S. C. Barton, M. A. Surani, K. Ryan, M. C. Nehls, V. Wilson, M. J. Evans, Eomesodermin is required for mouse trophoblast development and mesoderm formation. *Nature* **404**, 95–99 (2000).
36. M. Donnison, A. Beaton, H. W. Davey, R. Broadhurst, P. L'Huillier, P. L. Pfeffer, Loss of the extraembryonic ectoderm in Elf5 mutants leads to defects in embryonic patterning. *Development* **132**, 2299–2308 (2005).
37. K. Kusama, R. Bai, K. Imakawa, Regulation of human trophoblast cell syncytialization by transcription factors STAT5B and NR4A3. *J. Cell. Biochem.* **119**, 4918–4927 (2018).
38. A. Togayachi, T. Akashima, R. Ookubo, T. Kudo, S. Nishihara, H. Iwasaki, A. Natsume, H. Mio, J. Inokuchi, T. Irimura, K. Sasaki, H. Narimatsu, Molecular cloning and characterization of UDP-GlcNAc:lactosylceramide beta 1,3-N-acetylglucosaminyltransferase (beta 3Gn-T5), an essential enzyme for the expression of HNK-1 and Lewis X epitopes on glycolipids. *J. Biol. Chem.* **276**, 22032–22040 (2001).
39. Y. Tajiri, T. Igarashi, D. Li, K. Mukai, M. Suematsu, E. Fukui, M. Yoshizawa, H. Matsumoto, Tubulointerstitial nephritis antigen-like 1 is expressed in the uterus and binds with integrins in decidualized endometrium during postimplantation in mice. *Biol. Reprod.* **82**, 263–270 (2010).
40. E. Balta, R. Hardt, J. Liang, H. Kirchgessner, C. Orlik, B. Jahraus, S. Hillmer, S. Meuer, K. Hubner, G. H. Wabnitz, Y. Samstag, Spatial oxidation of L-plastin downmodulates actin-based functions of tumor cells. *Nat. Commun.* **10**, 4073 (2019).
41. Y. Tu, L. Zhang, L. Tong, Y. Wang, S. Zhang, R. Wang, L. Li, Z. Wang, EFhd2/swiprosin-1 regulates LPS-induced macrophage recruitment via enhancing actin polymerization and cell migration. *Int. Immunopharmacol.* **55**, 263–271 (2018).
42. J. Block, D. Breitsprecher, S. Kuhn, M. Winterhoff, F. Kage, R. Geffers, P. Duwe, J. L. Rohn, B. Baum, C. Brakebusch, M. Geyer, T. E. Stradal, J. Faix, K. Rottner, FMNL2 drives actin-based protrusion and migration downstream of Cdc42. *Curr. Biol.* **22**, 1005–1012 (2012).
43. L. R. Guerin, J. R. Prins, S. A. Robertson, Regulatory T-cells and immune tolerance in pregnancy: A new target for infertility treatment? *Hum. Reprod. Update* **15**, 517–535 (2009).
44. P. Jacquemin, V. Sapin, E. Alsat, D. Evain-Brion, P. Dolle, I. Davidson, Differential expression of the TEF family of transcription factors in the murine placenta and during differentiation of primary human trophoblasts in vitro. *Dev. Dyn.* **212**, 423–436 (1998).
45. R. A. Saxton, D. M. Sabatini, mTOR signaling in growth, metabolism, and disease. *Cell* **168**, 960–976 (2017).
46. R. Vento-Tormo, M. Efremova, R. A. Botting, M. Y. Turco, M. Vento-Tormo, K. B. Meyer, J. E. Park, E. Stephenson, K. Polanski, A. Goncalves, L. Gardner, S. Holmqvist, J. Henriksson, A. Zou, A. M. Sharkey, B. Millar, B. Innes, L. Wood, A. Wilbrey-Clark, R. P. Payne, M. A. Ivarsson, S. Lisgo, A. Filby, D. H. Rowitch, J. N. Bulmer, G. J. Wright, M. J. T. Stubbington, M. Haniffa, A. Moffett, S. A. Teichmann, Single-cell reconstruction of the early maternal-fetal interface in humans. *Nature* **563**, 347–353 (2018).
47. L. Przybyl, N. Haase, M. Golic, J. Rugor, M. E. Solano, P. C. Arck, M. Gauster, B. Huppertz, C. Emontzpohl, C. Stoppe, J. Bernhagen, L. Leng, R. Bucala, H. Schulz, A. Heuser, M. S. Weedon-Fekjaer, G. M. Johnsen, D. Peetz, F. C. Luft, A. C. Staff, D. N. Muller, R. Dechend, F. Herse, CD74-downregulation of placental macrophage-trophoblastic interactions in preeclampsia. *Circ. Res.* **119**, 55–68 (2016).
48. E. S. Taglauer, A. S. Trikhacheva, J. G. Slusser, M. G. Petroff, Expression and function of PDCD1 at the human maternal-fetal interface. *Biol. Reprod.* **79**, 562–569 (2008).
49. A. Habicht, S. Dada, M. Jurewicz, B. T. Fife, H. Yagita, M. Azuma, M. H. Sayegh, I. Guleria, A link between PDL1 and T regulatory cells in fetomaternal tolerance. *J. Immunol.* **179**, 5211–5219 (2007).
50. N. Sugino, S. Kashida, A. Karube-Harada, S. Takiguchi, H. Kato, Expression of vascular endothelial growth factor (VEGF) and its receptors in human endometrium throughout the menstrual cycle and in early pregnancy. *Reproduction* **123**, 379–387 (2002).
51. C. Weber, K. S. Weber, C. Klier, S. Gu, R. Wank, R. Horuk, P. J. Nelson, Specialized roles of the chemokine receptors CCR1 and CCR5 in the recruitment of monocytes and T_H1-like/CD45RO$^+$ T cells. *Blood* **97**, 1144–1146 (2001).
52. K. M. Lee, R. Danuser, J. V. Stein, D. Graham, R. J. Nibbs, G. J. Graham, The chemokine receptors ACKR2 and CCR2 reciprocally regulate lymphatic vessel density. *EMBO J.* **33**, 2564–2580 (2014).
53. T. Eisenberg, H. Knauer, A. Schauer, S. Buttner, C. Ruckenstuhl, D. Carmona-Gutierrez, J. Ring, S. Schroeder, C. Magnes, L. Antonacci, H. Fussi, L. Deszcz, R. Hartl, E. Schraml, A. Criollo, E. Megalou, D. Weiskopf, P. Laun, G. Heeren, M. Breitenbach, B. Grubeck-Loebenstein, E. Herker, B. Fahrenkrog, K. U. Frohlich, F. Sinner, N. Tavernarakis, N. Minois, G. Kroemer, F. Madeo, Induction of autophagy by spermidine promotes longevity. *Nat. Cell Biol.* **11**, 1305–1314 (2009).
54. J. Zhang, S. M. de Toledo, B. N. Pandey, G. Guo, D. Pain, H. Li, E. I. Azzam, Role of the translationally controlled tumor protein in DNA damage sensing and repair. *Proc. Natl. Acad. Sci. U.S.A.* **109**, E926–E933 (2012).

55. D. Benelli, S. Cialfi, M. Pinzaglia, C. Talora, P. Londei, The translation factor eIF6 is a Notch-dependent regulator of cell migration and invasion. *PLOS ONE* **7**, e32047 (2012).
56. V. Gandin, A. Miluzio, A. M. Barbieri, A. Beugnet, H. Kiyokawa, P. C. Marchisio, S. Biffo, Eukaryotic initiation factor 6 is rate-limiting in translation, growth and transformation. *Nature* **455**, 684–688 (2008).
57. A. Gandarillas, R. Molinuevo, N. Sanz-Gomez, Mammalian endoreplication emerges to reveal a potential developmental timer. *Cell Death Differ.* **25**, 471–476 (2018).
58. C. Cuman, E. Menkhorst, A. Winship, M. Van Sinderen, T. Osianlis, L. J. Rombauts, E. Dimitriadis, Fetal-maternal communication: The role of Notch signalling in embryo implantation. *Reproduction* **147**, R75–R86 (2014).
59. H. Kagawa, A. Javali, H. H. Khoei, T. M. Sommer, G. Sestini, M. Novatchkova, Y. ScholteOpReimer, G. Castel, A. Bruneau, N. Maenhoudt, J. Lammers, S. Loubersac, T. Freour, H. Vankelecom, L. David, N. Rivron, Human blastoids model blastocyst development and implantation. *Nature* **601**, 600–605 (2022).
60. V. V. Ignatova, P. Stolz, S. Kaiser, T. H. Gustafsson, P. R. Lastres, A. Sanz-Moreno, Y. L. Cho, O. V. Amarie, A. Aguilar-Pimentel, T. Klein-Rodewald, J. Calzada-Wack, L. Becker, S. Marschall, M. Kraiger, L. Garrett, C. Seisenberger, S. M. Holter, K. Borland, E. Van De Logt, P. Jansen, M. P. Baltissen, M. Valenta, M. Vermeulen, W. Wurst, V. Gailus-Durner, H. Fuchs, M. H. de Angelis, O. J. Rando, S. M. Kellner, S. Bultmann, R. Schneider, The rRNA m^6A methyltransferase METTL5 is involved in pluripotency and developmental programs. *Genes Dev.* **34**, 715–729 (2020).
61. X. C. Li, F. Jin, B. Y. Wang, X. J. Yin, W. Hong, F. J. Tian, The m6A demethylase ALKBH5 controls trophoblast invasion at the maternal-fetal interface by regulating the stability of *CYR61* mRNA. *Theranostics* **9**, 3853–3865 (2019).
62. S. Stigliani, G. Orlando, C. Massarotti, I. Casciano, F. Bovis, P. Anserini, F. M. Ubaldi, V. Remorgida, L. Rienzi, P. Scaruffi, Non-invasive mitochondrial DNA quantification on day 3 predicts blastocyst development: A prospective, blinded, multi-centric study. *Mol. Hum. Reprod.* **25**, 527–537 (2019).
63. H. Guo, P. Zhu, X. Wu, X. Li, L. Wen, F. Tang, Single-cell methylome landscapes of mouse embryonic stem cells and early embryos analyzed using reduced representation bisulfite sequencing. *Genome Res.* **23**, 2126–2135 (2013).
64. S. Gao, L. Yan, R. Wang, J. Li, J. Yong, X. Zhou, Y. Wei, X. Wu, X. Wang, X. Fan, J. Yan, X. Zhi, Y. Gao, H. Guo, X. Jin, W. Wang, Y. Mao, F. Wang, L. Wen, W. Fu, H. Ge, J. Qiao, F. Tang, Tracing the temporal-spatial transcriptome landscapes of the human fetal digestive tract using single-cell RNA-sequencing. *Nat. Cell Biol.* **20**, 721–734 (2018).
65. C. Trapnell, L. Pachter, S. L. Salzberg, TopHat: Discovering splice junctions with RNA-Seq. *Bioinformatics* **25**, 1105–1111 (2009).
66. S. Anders, P. T. Pyl, W. Huber, HTSeq—A Python framework to work with high-throughput sequencing data. *Bioinformatics* **31**, 166–169 (2015).
67. R. Satija, J. A. Farrell, D. Gennert, A. F. Schier, A. Regev, Spatial reconstruction of single-cell gene expression data. *Nat. Biotechnol.* **33**, 495–502 (2015).
68. N. C. Chung, J. D. Storey, Statistical significance of variables driving systematic variation in high-dimensional data. *Bioinformatics* **31**, 545–554 (2015).
69. E. Z. Macosko, A. Basu, R. Satija, J. Nemesh, K. Shekhar, M. Goldman, I. Tirosh, A. R. Bialas, N. Kamitaki, E. M. Martersteck, J. J. Trombetta, D. A. Weitz, J. R. Sanes, A. K. Shalek, A. Regev, S. A. McCarroll, Highly parallel genome-wide expression profiling of individual cells using nanoliter droplets. *Cell* **161**, 1202–1214 (2015).
70. I. Tirosh, B. Izar, S. M. Prakadan, M. H. Wadsworth 2nd, D. Treacy, J. J. Trombetta, A. Rotem, C. Rodman, C. Lian, G. Murphy, M. Fallahi-Sichani, K. Dutton-Regester, J. R. Lin, O. Cohen, P. Shah, D. Lu, A. S. Genshaft, T. K. Hughes, C. G. Ziegler, S. W. Kazer, A. Gaillard, K. E. Kolb, A. C. Villani, C. M. Johannessen, A. Y. Andreev, E. M. Van Allen, M. Bertagnolli, P. K. Sorger, R. J. Sullivan, K. T. Flaherty, D. T. Frederick, J. Jane-Valbuena, C. H. Yoon, O. Rozenblatt-Rosen, A. K. Shalek, A. Regev, L. A. Garraway, Dissecting the multicellular ecosystem of metastatic melanoma by single-cell RNA-seq. *Science* **352**, 189–196 (2016).
71. C. Trapnell, D. Cacchiarelli, J. Grimsby, P. Pokharel, S. Li, M. Morse, N. J. Lennon, K. J. Livak, T. S. Mikkelsen, J. L. Rinn, The dynamics and regulators of cell fate decisions are revealed by pseudotemporal ordering of single cells. *Nat. Biotechnol.* **32**, 381–386 (2014).

Acknowledgments: We thank F. Tang for technical assistance. The ISK cell line used in this work was a gift from H. Wang. **Funding:** This project was funded by the National Key Research and Development Program (2018YFC1004101, 2019YFA0801400, 2017YFA0103801, and 2018YFC1004000), the Strategic Priority Research Program of the Chinese Academy of Sciences (XDA16020703), the National Natural Science Foundation of China (81730038, 82001548, and 82125013), and the Fundamental Research Funds for the Central Universities–Peking University Clinical Scientist Program. **Ethics statement:** All studies concerning human embryos were reviewed and approved through an Embryo Research Oversight (EMRO) process, which was performed by the Reproductive Medicine Ethics Committee of Peking University Third Hospital (research license 2017SZ-070). All donors signed informed consent after they were well informed about the details of the study, including the usage of the donated samples, the benefits and risks of donation, the publication of sequencing data derived from the samples, and their right to withdraw the project at any time. All animal experiments were carried out according to the ethical guidelines of the Animal Care and Use Committee of Peking University. All of the studies and experiments were in accordance with the laws and policies effective in China. **Author contributions:** This project was conceived and coordinated by J.Q. and L.Y. The experiments were carried out by D.L., Y.R., P.Y., N.W., Q.L., C.Y., Z.Y., M.Y., J.W., J.Y., F.Z., Y.N., R.L., and X.Z. The bioinformatic analyses were performed by Yidong Chen. The sample collection was coordinated by Y.L. and Yuan Chen. H.-M.C. and P.C.K.L. provided important suggestions and helped modify the written report. The paper was written by D.L., Y.R., Y.C., L.Y., and J.Q. with input from all authors. **Competing interests:** The authors declare that they have no competing interests. **Data and materials availability:** All data needed to evaluate the conclusions in the paper are present in the paper and/or the Supplementary Materials. Our data have been deposited in the National Center for Biotechnology Information Gene Expression Omnibus (GEO) under accession number GSE133200. The raw human data have also been deposited in the National Genomics Data Center of the China National Center for Bioinformation (https://ngdc.cncb.ac.cn/gsa-human/) under accession number HRA000644. Codes for relevant analysis are available at https://github.com/jasminexiao/TE-related-code and https://zenodo.org/record/6732148.

Submitted 8 May 2021
Accepted 27 June 2022
Published 10 August 2022
10.1126/sciadv.abj3725